J Biol Inorg Chem (2016) 21:691–702
DOI 10.1007/s00775-016-1376-5

ORIGINAL PAPER

Role of N-terminal methionine residues in the redox activity of copper bound to alpha-synuclein

Esaú E. Rodríguez[1] · Trinidad Arcos-López[1] · Lidia G. Trujano-Ortiz[1] · Claudio O. Fernández[2] · Felipe J. González[1] · Alberto Vela[1] · Liliana Quintanar[1]

Received: 15 April 2016 / Accepted: 6 July 2016 / Published online: 15 July 2016

Abstract Amyloid aggregation of α-synuclein (AS) is one of the hallmarks of Parkinson's disease. The interaction of copper ions with the N-terminal region of AS promotes its amyloid aggregation and metal-catalyzed oxidation has been proposed as a plausible mechanism. The AS(1–6) fragment represents the minimal sequence that models copper coordination to this intrinsically disordered protein. In this study, we evaluated the role of methionine residues Met1 and Met5 in Cu(II) coordination to the AS(1–6) fragment, and in the redox activity of the Cu–AS(1–6) complex. Spectroscopic and electronic structure calculations show that Met1 may play a role as an axial ligand in the Cu(II)–AS(1–6) complex, while Met5 does not participate in metal coordination. Cyclic voltammetry and reactivity studies demonstrate that Met residues play an important role in the reduction and reoxidation processes of this complex. However, Met1 plays a more important role than Met5, as substitution of Met1 by Ile decreases the reduction potential of the Cu–AS(1–6) complex by ~80 mV, causing a significant decrease in its rate of reduction. Reoxidation of the complex by oxygen results in oxidation of the Met residues to sulfoxide, being Met1 more susceptible to copper-catalyzed oxidation than Met5. The sulfoxide species can suffer elimination of methanesulfenic acid, rendering a peptide with no thioether moiety, which would impair the ability of AS to bind Cu(I) ions. Overall, our study underscores the important roles that Met1 plays in copper coordination and the reactivity of the Cu–AS complex.

Keywords Copper · Alpha-synuclein · Electronic structure · EPR · Circular dichroism · DFT

Introduction

Parkinson's disease (PD) is the second most common neurodegenerative disorder in people above 60 years old [1]. This disorder is characterized by several symptoms: bradykinesia, resting tremor, rigidity and postural instability caused primarily by the loss of dopaminergic neurons in the *substantia nigra pars compacta* [2–4]. One of the hallmarks of PD is the presence of Lewy bodies, insoluble protein aggregates, composed mostly of a protein called alpha-synuclein (AS) [4]. AS is found in Lewy bodies in an amyloid aggregate form with different chemical modifications, including nitration, phosphorylation, ubiquitination, and truncation [5]. Although, the molecular mechanism of aggregation in AS is still unknown, there is evidence that metal ions play a crucial role. Indeed, levels of metals in the PD brain are altered, as compared to healthy brain: total iron is increased by 31–35 % while copper is reduced by 34–45 % in the substantia nigra [6].

AS is a small, presynaptic, intrinsically disordered protein found in many vertebrates [7]. The physiological role of AS is still unclear, but it has been proposed that it binds

Electronic supplementary material The online version of this article (doi:10.1007/s00775-016-1376-5) contains supplementary material, which is available to authorized users.

✉ Liliana Quintanar
lilianaq@cinvestav.mx

[1] Department of Chemistry, Centro de Investigación y de Estudios Avanzados (Cinvestav), Av. Instituto Politécnico Nacional 2508, 07360 Mexico City, Mexico

[2] Max Planck Laboratory for Structural Biology, Chemistry and Molecular Biophysics of Rosario (MPLbioR, UNR-MPIbpC) and Instituto de Investigaciones para el Descubrimiento de Fármacos de Rosario (IIDEFAR, UNR-CONICET), Universidad Nacional de Rosario, Ocampo y Esmeralda, S2002LRK Rosario, Argentina

to membranes via a mechanism that involves its N-terminus adopting an alpha helix conformation [8, 9]. The location of AS and its interaction with membranes could be related with accumulation of synaptic vesicles and promotion of presynaptic SNARE-complex assembly [10]. AS has also been reported to interact with a large number of proteins that might regulate its activity, such as synphilin, which is proposed to promote its aggregation [11], or its homolog beta-synuclein which is known to inhibit its aggregation [12]. The primary structure of AS can be divided in three characteristic regions: the N-terminus (residues 1–60); the hydrophobic and fibrillogenic non-amyloid component (NAC, 61–95) and the C-terminal region (96–140), which is rich in Pro, Glu and Asp residues. In its native monomeric state, AS adopts a random coil conformation [13, 14]. Five mutations in the protein sequence have been shown to cause early onset forms of PD and modify the aggregation of AS in vitro: A30P [15], E46K [16], A53T [17], G51D [18] and H50Q [19].

An early pioneer study showed that several metal ions, such as Al(III), Fe(III), and Cu(II), can accelerate the fibrillation of AS in vitro [20]. Indeed, a detailed NMR study showed that metal cations can interact with the acidic C-terminal domain of AS, causing protein aggregation. However, Cu(II) is the most effective ion in promoting AS oligomerization [21]. Copper binding to AS has been exhaustively investigated using a wide range of spectroscopic tools in relevant physiological conditions [22]. Unlike other metal ions, Cu(II) displays two distinct and specific interactions with the N-terminal domain of AS. The highest affinity Cu(II) binding site displays an apparent $K_d = 0.2 \pm 0.02$ μM (corresponding to a conditional $K_d = 0.1$ nM). This apparent binding affinity for Cu(II) ions is comparable to that of the amyloid precursor protein ($K_d = 0.01$ μM), the β-amyloid peptide ($K_d = 0.3$–0.4 μM), and the octarepeat domain of the human prion protein ($K_d = 0.1$–10 μM) [21]. AS and copper are highly abundant in brain tissue, AS accounts for approximately 1 % of the total protein content in the striatum [23], while altered copper levels are reported in PD [24, 25]. Thus, interactions of copper ions with AS are likely to occur in vivo, especially under adverse conditions.

The highest affinity Cu(II) binding site in AS is located at the N-terminal region, involving the amino NH_2 group of Met1, the deprotonated amide and the carboxylate moiety of Asp2, and a water molecule, forming a 2N2O equatorial coordination mode, as demonstrated previously by detailed spectroscopic studies [26, 27]. It has also been demonstrated that the short AS fragment 1–6 contains the essential residues to form the Cu(II)–AS complex, as described in the full protein [26, 27]. Thus, although the role of Met residues in Cu(II) coordination as potential axial ligands is still not clear, AS(1–6) is a useful model for the highest affinity Cu(II) binding site at the N-terminal region of AS. Copper can also bind to His50, yet with a lower affinity (apparent $K_d = 30$ μM), as compared to the AS(1–6) site. An equatorial 3NO coordination mode has been proposed for the His50 site, possibly involving deprotonated backbone amides from His50 and Val49, and a water molecule or backbone carbonyl [28]. Alternatively, it has been recently proposed that His50 may also be involved in the Cu(II) complex at the N-terminal end of the protein, replacing the water ligand [29].

Another feature of PD is related to the oxidative stress, defined as a disturbance in the balance between the production of reactive oxygen species (ROS) and antioxidant defenses in the cell. Protein oxidation has been implicated in several disorders involving oxidative stress, including Alzheimer's disease, PD, dementia with Lewy bodies, Huntington's disease, amyotrophic lateral sclerosis, diabetes, and amyloidosis [30–32]. Exogenous native AS at low concentrations protects neuronal cells against cellular stress conditions [33], however, the process of aggregation of AS from monomers, via oligomeric intermediates into amyloid fibrils is considered the disease-causative toxic mechanism. It has been demonstrated in vivo that oligomers of AS are more toxic than fibrils [34], while the mechanism of neurotoxicity might implicate the formation of hydrogen peroxide [35]. A working hypothesis is that the redox active Cu–AS complexes could generate ROS and cause oxidative damage to the protein (i.e. site-specific oxidation, dityrosine cross-linking, protein truncation), which in turn would lead to aggregation. Thus, site-specific oxidation, dityrosine cross-linking and fragmentation of AS mediated by AS–Cu interactions have been investigated [36–38]. It is known that methionine oxidation inhibits AS fibrillation and leads to the formation of soluble oligomers [39, 40]. The oxidation of methionine plays an important role in vivo, during biological conditions of oxidative stress, as well as for protein stability in vitro [41–43]. This observation is in agreement with previous reports, indicating that Met is one of the preferred targets in proteins under conditions of oxygen, hydrogen peroxide or site-specific metal-catalyzed oxidation. AS has four Met residues, two of them (Met1 and Met5) are at the N-terminus and the other two (Met116 and Met127) are in C-terminus. Although the mechanism of Met oxidation is unclear, the oxidation of such residues in AS has been described [36, 37, 40, 44].

Copper-catalyzed oxidation processes have been implicated in AS fibril formation, triggering structural studies of Cu(I) bound to AS. Recent NMR studies revealed the presence of a high affinity binding site (apparent $K_d = 20$ M) for Cu(I) involving Met1 and Met5 [36, 37, 45], while lower affinity sites have been identified at His50 and the Met116 and Met127 residues at the C-terminus [36]. A recent XAS study also

suggests the involvement of Asp2 and a water molecule in the coordination sphere of the Met1/Met5 Cu(I) binding site [46]. Similar to the case of Cu(II), the highest affinity binding site for Cu(I) in AS can be modeled by the peptide AS(1–6), which contains the essential residues to form this Cu(I)–AS complex [36]. Thus, AS(1–6) is a good model to study the redox activity of the Cu–AS complex.

In this study, we have evaluated the role of the Met residues (Met1 and Met5) in Cu(II) coordination to the AS(1–6) fragment, using spectroscopic and theoretical tools. We have also investigated the role of these Met residues in the redox activity of the Cu–AS(1–6) complex, particularly its reduction by ascorbate, and its reoxidation by oxygen, which promotes copper-catalyzed oxidation.

Materials and methods

Peptide synthesis and reagents

AS peptide fragments ^{1}MDVFMK^{6} [AS(1–6)] and its Met to Ile variants ^{1}IDVFMK^{6} (M1I), ^{1}MDVFIK^{6} (M5I), and ^{1}IDVFIK^{6} (M1I/M5I) were synthesized in solid-phase (Rink amide resin) using F-moc chemistry [47, 48]. They were purified by reverse phase high-performance liquid chromatography (HPLC, Waters Delta 600) and characterized by electrospray ionization mass spectrometry (Agilent ESI-TOF) (Figure S1). Peptides were amidated at the C-terminal carboxylate group, while the α-NH_2 terminal was left unmodified. 9-Fluorenylmethoxycarbonyl (Fmoc) protected amino acids and resins were obtained from Novabiochem (Merck). Water was purified to a resistivity of 18 MΩ/cm using a Millipore deionizing system. Copper (II) sulfate was used in all experiments.

Preparation of Cu–AS complexes

Lyophilized peptides were dissolved in 20 mM 3-(*N*-morpholino) propanesulfonic acid (MOPS) buffer, 100 mM NaCl, at pH 7.5. The absorption extinction coefficient at 214 nm for the peptides was determined using a calibration curve prepared in this buffer, and the value of 11,500 cm^{-1} M^{-1} was used to determine peptide concentration in all experiments. Final concentration for spectroscopic and kinetics studies was 0.3 mM. Cu(II)–peptide complexes were prepared by adding copper (II) sulfate in ratio 1:1. Peptide samples for EPR spectroscopy were prepared in the same buffer mixture with 50 % glycerol to achieve adequate glassing. The addition of glycerol has no effect in the structure of the Cu(II)–peptide complexes, as evaluated by absorption and CD spectroscopy.

Electronic absorption and circular dichroism spectroscopy

Room-temperature absorption and circular dichroism (CD) spectra in the UV–visible region were recorded using an Agilent 8453 diode array spectrometer and a Jasco J-815 CD spectropolarimeter, using a scan speed of 100 nm/min, a time constant of 0.5 s and a bandwidth of 2 nm. Three scans were accumulated. Spectra were recorded in a 1 cm path length quartz cell.

Electron paramagnetic resonance spectroscopy

Cu(II)–peptide complexes were analyzed by electron paramagnetic resonance (EPR) at 150 K, using an X-band EMX Plus Bruker EPR spectrometer, with an ER 041 XG microwave bridge and an ER 4102ST cavity. The following conditions were used: microwave power, 10 mW; modulation amplitude, 5 G; modulation frequency, 100 kHz; time constant, 327 ms; conversion time, 82 ms; and averaging over 12 scans.

Electronic structure calculations

The full AS(1–6) sequence, i.e. MDVFMK, was used in all models, with an amidated C-terminus, and a N-terminus without any modification. To build each set of models, different starting conformations of the peptide were tested: alpha helix (a), beta-sheet (b), turn (t), and extended (e) conformations. Eight different models were built, the numbers 4 and 5 denote tetra- and penta-coordinated models, respectively. Letters a, b, t and e indicate the initial peptide conformation, and S1 and S5 denote if the axial sulfur ligand corresponds to Met1 or Met5, respectively. Each Cu(II)–peptide complex was constructed in Molden [49], and the structures have a total of 111 atoms. Their electronic structure was obtained using spin-unrestricted Kohn–Sham Theory (UKS) within the linear combination of Gaussian-type orbitals to solve the Kohn–Sham equations (LCGTO-KS) [50] as implemented in the deMon2k code [51], which uses the variational fitting of the Coulomb energy to avoid the calculation of 4-center integrals, at the expense of introducing an additional auxiliary basis set. All structures had a spin multiplicity of two (doublet) and were fully optimized without any geometry constraints at local level (LDA) with the Dirac [52]—VWN [53] exchange–correlation functional and then with the generalized gradient approximation (GGA) exchange–correlation functional PBE [54], using a double-ζ plus polarization (DZVP) [55] orbital basis set and a GEN-A2 [56, 57] auxiliary basis set. A frequency analysis was done for all the stationary points located in the potential energy surface with the PBE functional. It is important to mention that the

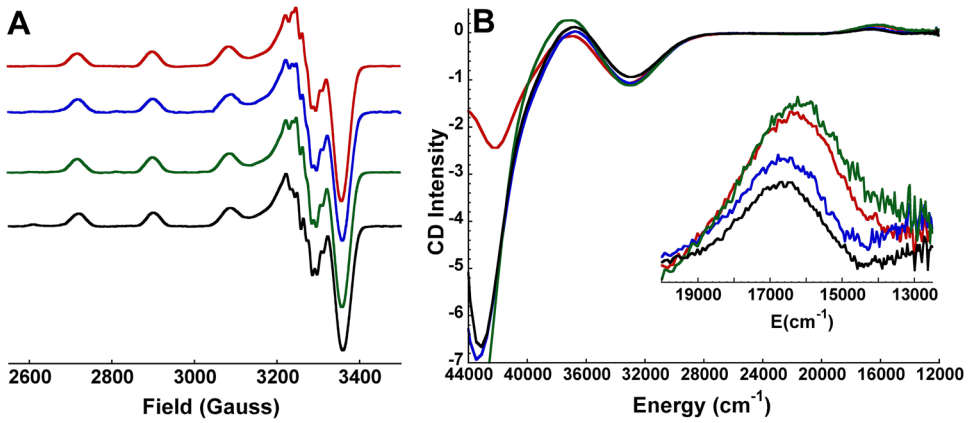

Fig. 1 EPR (**a**) and CD (**b**) spectra of Cu(II) complexes with AS(1–6) (*red*), and its Met to Ile variants: M1I (*blue*), M5I (*green*), and M1I/M5I (*black*). In all cases, the Cu(II):peptide ratio was 0.9:1.0, and the total peptide concentration was 0.3 mM, using MOPS buffer pH 7.5

exchange–correlation energy and potential were evaluated using the auxiliary density. The optimized structures were used to calculate the EPR parameters (**g** and **A** tensors) with the ORCA program [58], using the global non-empirical hybrid functional PBE0 [59] with the CP basis [60] for copper and the DGAUSS basis [55] in all other atoms. Solvent effects were included using the implicit solvation model COSMO in ORCA [61, 62].

Cyclic voltammetry (CV)

CV experiments were performed at room temperature using a Voltalab potentiostat PGZ 100 in a three electrode arrangement with a Ag/AgCl reference electrode, a platinum wire as the auxiliary electrode, and a glassy carbon electrode (GCE, 3 mm diameter) as the working electrode; the latter was polished with 0.3 μm alumina powder on a cloth polishing pad and washed with water and ethanol under sonication. Phosphate buffer (10 mM) was used with Na_2SO_4 (50 mM) as the supporting electrolyte at pH 7.4. Argon was used to maintain inert conditions during the experiments. Total peptide concentration was 0.3 mM with Cu(II) [1:1], while the potential scan rate was 5 mVs^{-1}.

Reduction kinetics of the Cu(II)–peptide complexes

The reduction of Cu(II)–peptides complexes by ascorbate was performed under anaerobic conditions. Cu(II)–peptide complexes in 20 mM MOPS buffer pH 7.5 were degassed in a Schlenk line, under a high purity nitrogen atmosphere. The degassed complexes were placed in an anaerobic 1 cm path length quartz cell. Upon addition of 16 equiv of L-(+)ascorbate [the minimal amount of ascorbate needed to achieve full reduction of the AS(1–6) complex], the intensity of the characteristic d–d transition band (610 nm) in the UV–Vis absorption spectrum was followed over time. The solution was purged with high purity nitrogen during the course of the experiment.

Reoxidation of the Cu(I)–AS(1–6) complex and HPLC-mass spectrometry analysis

Reduction of the Cu(II)–AS(1–6) and its Met to Ile variants were performed as described above. The reaction of the Cu(I)-complexes with oxygen was initiated by adding oxygen-saturated buffer at 4 °C (10 % volume), and the reaction was monitored by UV–Vis absorption spectroscopy, using an Agilent 8453 diode array UV–Vis spectrometer. After reoxidation, the samples were treated with ethylenediaminetetraacetic acid (EDTA) and injected into an Eclipse XDB-C18 column (4.6 × 150 mm, 5 μm) at 25 °C, with a flow rate of 0.5 mL/min, using an HPLC chromatograph coupled to an ESI-TOF spectrometer (Agilent). The capillary voltage was 3500 V, and degassing temperature was 300 °C.

Results and discussion

Spectroscopic study of Cu(II)–AS peptide complexes

To evaluate the role of Met1 and Met5 in Cu(II) coordination at the N-terminal site in AS, we studied several Met to Ile variants of the AS(1–6) peptide: M1I, M5I and M1I/M5I. Titrations of these peptides with Cu(II), as followed by CD, show that they form complexes with 1:1 Cu:peptide ratio, in a similar fashion as the AS(1–6) peptide. A comparison of the EPR spectra of all Cu(II) complexes shows identical signals, regardless of the presence of Met residues (Fig. 1a). One single set of EPR signals with parameters $g_z = 2.25$ and $A_z = 184$ G is observed in all cases. These parameters have been associated to Cu(II) bound to AS(1–6) with an equatorial coordination mode 2N2O, as previously described [26]. Similarly, the CD spectra for these complexes are almost identical (Fig. 1b), showing a positive ligand field transition at 16,400 cm^{-1} (610 nm) and negative ligand to metal charge transfer (LMCT) at

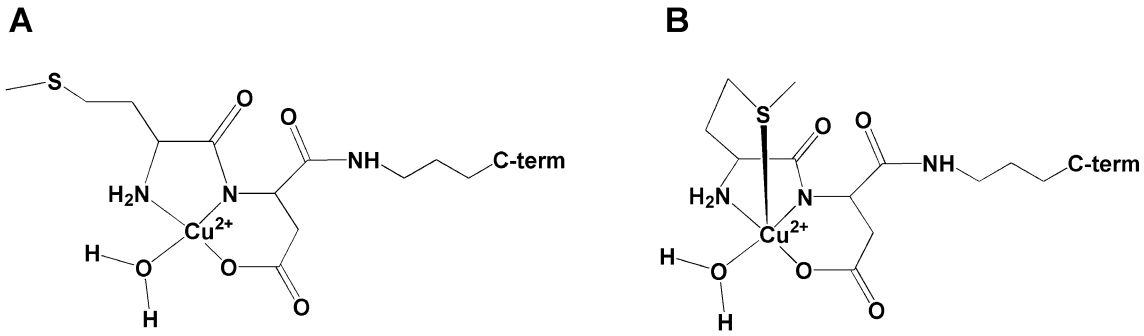

Scheme 1 Proposed Cu(II) coordination modes for Cu–AS(1–6) complexes: 2N2O (**a**) and 2N2OS with Met1 as axial ligand (**b**)

33,000 cm^{-1} (303 nm), which has been assigned to a deprotonated amide to Cu(II) LMCT transition [27]. Furthermore, a second LMCT band is observed at higher energy (43,000 cm^{-1}; 233 nm), which falls in the range for NH_2 to Cu(II) LMCT transitions [63]. Only a small decrease in intensity at the ligand field transition at 16,650 cm^{-1} is observed for the M1I and M1I/M5I variants, as compared to the spectrum of the AS(1–6) and M5I complexes. This small change might be due to a difference in the ligand field strength and/or decrease in covalency of the Cu(II) complex, which is clearly associated to the absence of Met1. This observation suggests that Met1 may play a role as axial ligand or as part of the second sphere coordination shell of Cu(II) bound to AS(1–6).

Overall, these spectroscopic results indicate that the equatorial coordination shell for Cu(II) bound to AS(1–6) is not affected significantly by Met to Ile substitutions at positions 1 and 5, and Met5 definitely does not participate in Cu(II) coordination at all. However, we cannot discard the possibility that Met1 might participate as an axial ligand or as an important residue in the second sphere coordination shell (Scheme 1).

Electronic structure calculations of the Cu(II)–AS(1–6) complexes

UKS calculations were performed to evaluate the two coordination models for the Cu(II)–AS(1–6) complex shown in Scheme 1. The equatorial ligands in both models are: the $-NH_2$ group of Met1, the deprotonated amide nitrogen from Asp2 (N^-_{D2}), the carboxylate side chain oxygen from Asp2 (β-COO^-_{D2}), which enables the formation of (5,6)-membered joined chelate rings, and a water molecule, leading to a 2N2O equatorial coordination shell. In some models, a sulfur atom from either Met1 or Met5 participates as an axial ligand, yielding a penta-coordinated complex 2N2O1S. To build each set of models, different starting conformations of the peptide were tested: alpha helix (a), beta-sheet (b), turn (t), and extended (e) conformations. Figure 2 shows the eight different models that are evaluated; notation is given in "Materials and methods". The optimized structural parameters at local (VWN) and GGA (PBE) levels are reported in Table S1, and the PBE structures are shown in Fig. 2. Regardless of the exchange–correlation functional used, the coordination geometry in the 4a, 4t, 4b and 4e models is square planar; and the structures contain two bonds with distances >2 Å ($Cu–NH_2$ and $Cu–O_w$) and two bonds with distances <2 Å ($Cu–N^-_{D2}$ and $Cu–O_{D2}$). These metal–ligand distances from our tetra-coordinated optimized structures are in agreement with the Cu–ligand bond distances previously obtained by QM/MM simulations [27]. In the models 5S1t, 5S1a, 5S1b and 5S5t, which contain a sulfur atom in the axial position, the equatorial bond distances are larger than in the tetra-coordinated structures, and show either tetrahedral or square pyramidal geometries.

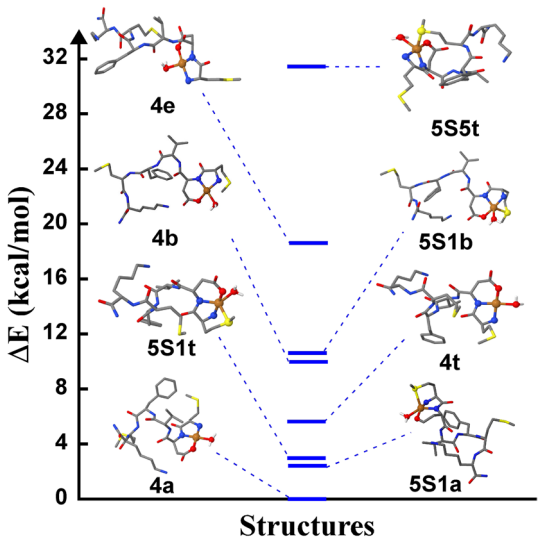

Fig. 2 Energy diagram of optimized structures of the tetra- and penta-coordinated models for the Cu(II)–AS(1–6) complex. For clarity, most of H atoms are not shown

Table 1 EPR parameters of optimized structures of the tetra- and penta-coordinated models (2N2O and 2N2O1S) for the Cu(II)–AS(1–6) complex

ID	**g** tensor			**A** tensor		
	g_{xx}	g_{yy}	g_{zz}	A_{xx}	A_{yy}	A_{zz}
4a	2.051	2.053	2.182	−55.44	−65.19	−632.12
5S1t	2.017	2.112	2.189	−154.69	157.95	−471.34
5S1a	2.050	2.054	2.220	−36.56	74.97	−530.33
4t	2.045	2.055	2.184	−25.05	−59.31	−614.61
5S1b	2.023	2.106	2.192	109.90	−152.75	−505.62
5S5	2.032	2.088	2.192	75.73	−113.44	−522.18
Experimental[a]	2.051	2.059	2.250	57.00	24.00	567.00

The **g** and **A** tensors were calculated with the PBE0 functional. The **A** tensor components are reported in MHz. The structures are listed in ascending order of their relative energies

[a] Values obtained from an EPR simulation of the experimental spectrum, as reported in Ref. [27]

Among the lowest energy structures, with relative energies smaller than 5 kcal/mol (Table S2), two of them are tetra-coordinated (4a and 4t) and two others contain the sulfur atom from Met1 in the axial position (5S1t and 5S1a). Overall, models with alpha helix (a) or turn (t) conformations have lower energies than models built with beta-sheet (b) or extended (e) conformations. On the other hand, it was not possible to build penta-coordinated models with Met5 as axial ligand starting from extended or beta-sheet conformations; while in the alpha helix conformation, the Met5 axial ligand came out of the coordination sphere upon geometric optimization. Thus, only one penta-coordinated model with Met5 as axial ligand (5S5t) was obtained, and it corresponds to the highest energy structure with a relative energy of ~30 kcal/mol. These results indicate that Met5 cannot participate as axial ligand for Cu(II) in the Cu(II)–AS(1–6) complex.

Next, the EPR parameters for selected Cu(II) models (4a, 5S1t, 5S1a, 4t, 5S1b and 5S5t) were calculated (Table 1). Previously reported EPR parameters for the Cu(II)–AS(1–6) complex [27], obtained from a simulation of the experimental data, are listed in Table 1 for comparison. Differences between calculated and experimental **g** and **A** values in the order of 0.03 ppm and 50 MHz, respectively, are usually considered acceptable for this type of calculations [64–68]. The 5S1a model is the only one that fulfills these criteria, while the 4t model is overall in good agreement with the experimental data, except for the g_z value. It should be noted though that the inclusion of explicit water molecules in the 4t model significantly improves the g_z and A_z values, bringing them closer to the experimental numbers (Figure S2). Overall, our electronic structure calculations indicate that the specific interaction of either a sulfur atom from Met1 or solvating water molecules in the axial position is necessary to reproduce the experimental EPR parameters. Thus, both, the tetra-coordinated 2N2O and the penta-coordinated 2N2O1S with axial Met1, are plausible coordination models for the Cu(II)–AS(1–6) complex and these two species might coexist. Removal of Met1 would not be expected to impact the EPR parameters significantly, while it might affect the ligand field transitions, as observed by CD (vide supra).

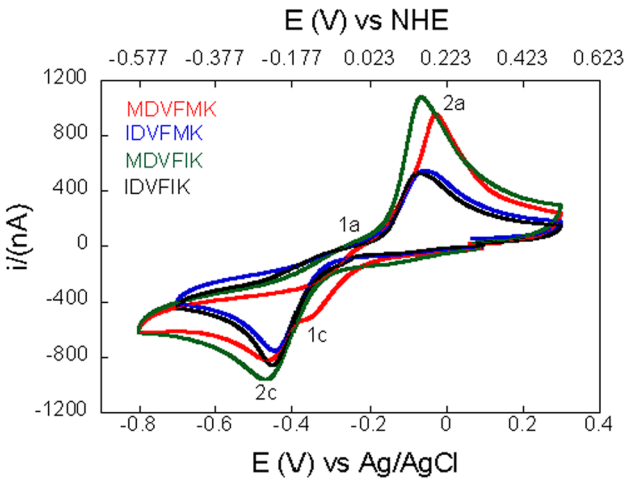

Fig. 3 Cyclic voltammetry of Cu complexes with AS(1–6) (*red*), and its Met to Ile variants: M1I (*blue*), M5I (*green*), and M1I/M5I (*black*), collected at a scan rate of 5 mV/s. *Anodic peaks* are indicated as *1a* or *2a*, while *cathodic peaks* correspond to *1c* or *2c*

Cyclic voltammetry of Cu–AS(1–6) complexes

Cyclic voltammetry of the different Cu(II)–peptide complexes was performed at pH 7.4 (Fig. 3). The electrochemical behavior of the Cu(II)–AS(1–6) complex (red line) displays two consecutive reduction peaks: $E_{pc}^{(1)} \approx -0.365$ and $E_{pc}^{(2)} = -0.461$ V vs Ag/Ag^+ (−0.142 and −0.238 V vs NHE and labeled as 1c and 2c, respectively), that are related to two overlapping oxidation peaks: $E_{pa}^{(1)} \approx -0.101$ and $E_{pa}^{(2)} = -0.024$ V vs Ag/Ag^+ (0.122 and 0.199 V vs NHE and labeled as 1a and 2a, respectively).

The observation of these two sets of peaks indicates the occurrence of two different redox processes. Upon any of the Met to Ile substitutions, the peaks at $E_{pc}^{(1)} \approx -0.365$ and $E_{pa}^{(1)} \approx -0.101$ V vs Ag/Ag^+ disappear, yielding very similar voltammograms. This result suggests that the redox process responsible for these two signals requires the presence of both, Met1 and Met5 residues. The spectroscopic characterization performed in this study indicates that Met1 can participate as an axial ligand to Cu(II), while previous NMR studies of the Cu(I)–AS complexes indicate that both, Met1 and Met5 residues participate in Cu(I) coordination [36, 37]. Thus, it is plausible to assign the cathodic peak at $E_{pc}^{(1)} \approx -0.365$ V vs Ag/Ag^+ (−0.142 V vs NHE) to the reduction of the Cu(II)–AS(1–6) complex to a Cu(I) species bound to both Met residues.

Overall, the voltammograms for the Cu complexes that contain Met1, i.e. Cu(II)–AS(1–6) (red line) and Cu(II)–AS(1–6)M5I (green line), display very broad reduction peaks that are almost identical: $E_{pc}^{MDVFMK} = -0.461$ and $E_{pc}^{MDVFIK} = -0.467$ V vs Ag/Ag^+ (−0.238 and −0.244 V vs NHE, respectively; labeled as 2c in each trace in Fig. 3). Both peaks display a half-peak width of about 67 mV, which indicates that the rate of reduction of these complexes is slow. This value of half-peak width is intermediate between the theoretical values for a fast electron transfer (Nernstian, 59 mV) and a slow electron transfer step (electrochemically irreversible, 95.6 mV) [69]. Considering that the cathodic and anodic peaks are quite far apart (405–433 mV), it can be proposed that the Cu(II)–AS(1–6) and Cu(II)–AS(1–6)M5I complexes are reduced following a quasi-reversible electron transfer step followed by a coupled chemical reaction that can be considered as the reorganization in the coordination mode related to the stabilization of the Cu(I) complexes. For these complexes, containing Met1, one could assume that two possible Cu(II) species would form: 2N2O or 2N2O1S with Met1 as an axial ligand. In both cases, a large reorganization would be needed to yield a reduced Cu(I) species with either both Met residues as ligands [for AS(1–6)] or only Met1 residue in the Cu(I) coordination shell [for AS(1–6)M5I]. In either case, at least one Met residue needs to come into the coordination sphere to stabilize the Cu(I) species.

On the other hand, the voltammograms of the complexes that lack Met1, i.e. Cu(II)–AS(1–6)M1I (black line) and Cu(II)–AS(1–6)M1I/M5I (blue line) show an identical pattern (Fig. 3), where the reduction peaks are observed at around −0.44 V: $E_{pc}^{IDVFMK} = -0.444$ and $E_{pc}^{IDVFIK} = -0.449$ V vs Ag/Ag^+ (−0.221 and −0.226 V vs NHE, respectively; labeled as 2c in each trace in Fig. 3). These peaks appear at less negative values and display a sharper shape than those obtained for the complexes bearing the Met1 residue. Additionally, the electron transfer kinetics for these complexes seem to be faster than in the case of the Cu(II)–AS(1–6) and Cu(II)–AS(1–6)M5I complexes, as revealed by a higher value of the half-peak width (62 mV). In the absence of Met1, the only plausible starting Cu(II) complex would be a 2N2O coordination mode, which would either be reduced to a Cu(I) species with only nitrogen or oxygen ligands [as in the case of AS(1–6)M1I/M5I], or it might recruit Met5 as a Cu(I) ligand [as in the case of AS(1–6)M1I], although such process would require a large reorganization of the peptide chain. Since in both cases, the voltammogram is practically identical, it is likely that the former process is responsible for the observed cathodic peak, yielding an electrochemical-chemical mechanism.

Overall, the cyclic voltammetry experiments demonstrate that the Met residues play an important role in the reduction and reoxidation processes of the Cu–AS(1–6) complex, which will be next evaluated in the context of chemical processes.

Reduction kinetics of Cu(II)–AS(1–6) complexes

The role of the methionine residues 1 and 5 in the reduction kinetics of the Cu(II)–AS(1–6) complex were evaluated. Reduction of the Cu(II)–AS(1–6) complex and its Met to Ile variants by ascorbate was examined at pH 7.5 in 20 mM MOPS buffer under anaerobic conditions, by electronic absorption spectroscopy. Absorption intensity at 610 nm, the characteristic d–d band in these complexes, was monitored as a function of time after addition of a 16-fold excess of reductant. Plots of the absorption traces for each Cu(II)–peptide complex are shown in Fig. 4. The reduction of the Cu(II)–AS(1–6) complex by ascorbate was almost complete 120 min after the addition of the reductant, the absorption intensity at 610 nm was decreased by 93 % (Fig. 4, red). Similarly, the reduction of the Cu(II)–AS(1–6)M5I variant occurs to a similar extent (84 %, Fig. 4, green). However, for the complex that lacks Met1, i.e. Cu(II)–AS(1–6)M1I, the reduction of the complex becomes more difficult, and only 45 % of the complex is reduced (Fig. 4, blue). Most strikingly, when both Met residues have been replaced by Ile, the Cu(II)–peptide complex cannot be reduced by ascorbate (Fig. 4, black) at all, even when a 50-fold excess of reductant is added. These results clearly indicate that the Met residues are essential for the reduction of this complex, and particularly, Met1 seems to play a more important role than Met5.

Based on the anaerobic reduction of the Cu(II)–AS(1–6) complexes by ascorbate, estimates for their reduction potential may be obtained (see Supporting Information). The reduction potential for the Cu(II/I)–AS(1–6) complex is estimated to be 82 mV, for the Cu(II/I)–AS(1–6)M5I variant the potential would be 57 mV, while the M1I

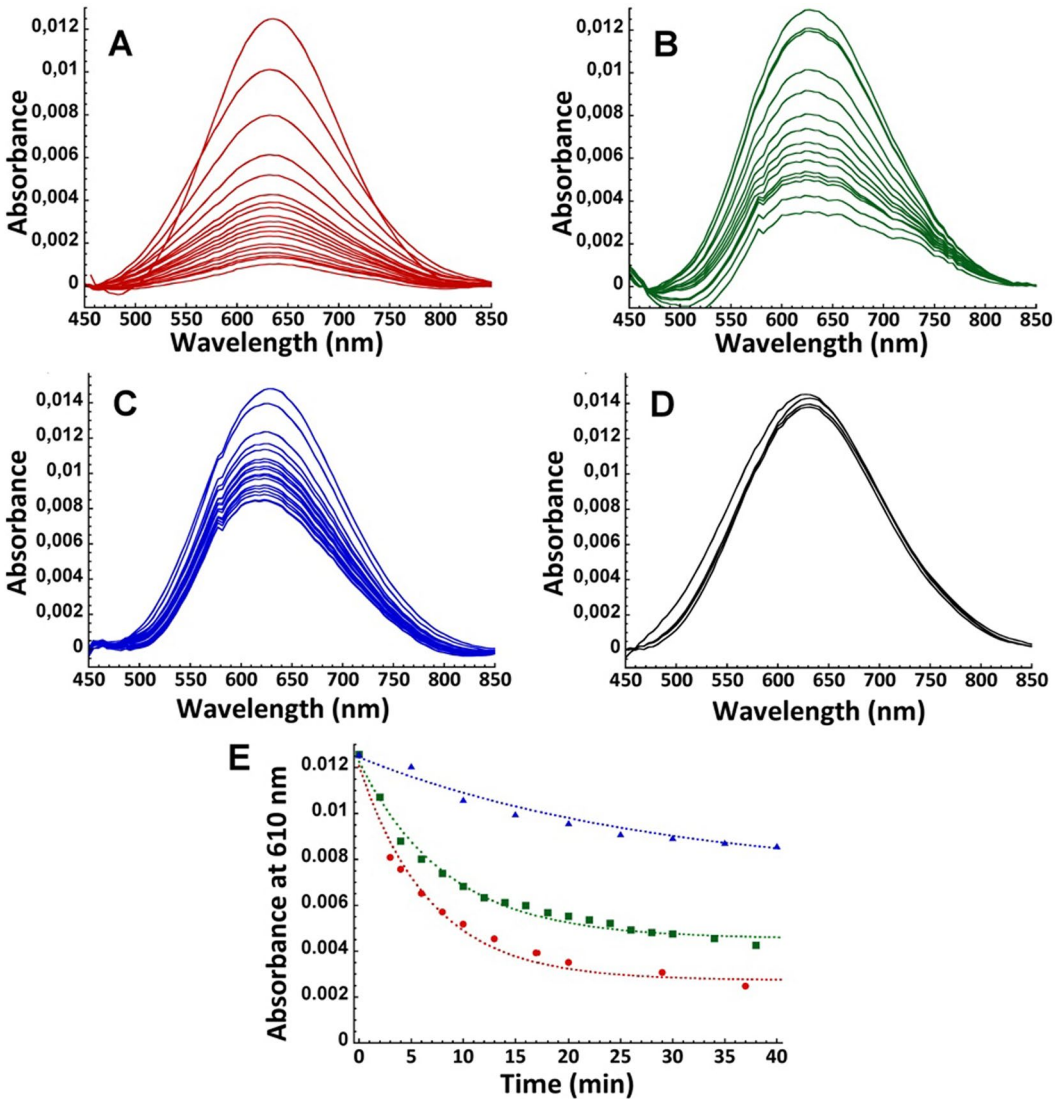

Fig. 4 Absorption spectra in the d–d region for the Cu(II)–AS(1–6) complex (**a**), and its Met to Ile variants: M5I (**b**), M1I (**c**), and M1I/M5I (**d**), as a function of time, upon addition of 16 equiv. of ascorbate. Representative kinetic traces for the reduction of the Cu(II) complexes with AS(1–6) complex (*red*), AS(1–6)M5I (*green*), and AS(1–6)M1I (*blue*) are shown in **e**; data were fitted to a single exponential fit (*lines*), yielding the rate constants listed in Table 2. No reduction of the Cu(II)AS(1–6)M1I/M5I was observed (**d**). In all cases, the Cu(II):peptide ratio was 0.9:1.0, and the total peptide concentration was 0.3 mM, using MOPS buffer pH 7.5. Experiments were performed under anaerobic conditions

substitution causes the largest drop in reduction potential, as an estimate of 1.4 mV is obtained for the reduction potential of the Cu(II/I)–AS(1–6)M1I complex. The drastic decrease in reduction potential of the Cu(II/I)–AS(1–6) complex upon replacement of Met1 by Ile is consistent with a decreased affinity for Cu(I), as detected by a recent NMR study [37]. The binding affinity of AS(1–6) for Cu(I) was determined to have an apparent K_d of 20 μM, while that for the AS(1–6)M1I peptide increased to ≥500 μM. Using a thermodynamic cycle scheme, relating the reduction potential of the Cu–AS(1–6) complex to that of free Cu and the relative affinities of the AS(1–6) peptide for Cu(II) and Cu(I) ions, it can be estimated that the observed drop in binding affinity for Cu(I) caused by the M1I mutation would translate in a decrease of 82 mV in the reduction potential of the complex (see Supporting Information). This is in excellent agreement with our experimental estimates for the reduction potentials of the Cu–AS(1–6) complexes, revealing a decrease of 80.6 mV for the M1I variant.

For each complex, the kinetic traces of reduction were fitted to a pseudo-first order decay model (Fig. 4), yielding the reduction rates (k_{obs}) listed in Table 2. The rates of reduction of the Cu(II) complexes with the AS(1–6) and AS(1–6)M5I peptides are almost identical (0.120 ± 0.016

Table 2 First order reduction rate constants for Cu(II)–AS(1–6) complexes

Cu complex	k_{obs} (min^{-1})
MDVFMK-Cu(II)	0.120 ± 0.016
MDVFIK-Cu(II)	0.100 ± 0.005
IDVFMK-Cu(II)	0.050 ± 0.001
IDVFIK-Cu(II)	No reduction

Standard deviation from at least triplicate experiments is provided

and 0.10 ± 0.054 min^{-1}, respectively). However, replacement of Met1 by Ile leads to a significant decrease in reduction rate: $k_{obs} = 0.050 \pm 0.001$ min^{-1}, strongly suggesting that Met1 plays a key role in the reduction of the Cu(II)–AS(1–6) complex. Considering that the M1I substitution causes a significant decrease in the reduction potential of the Cu–AS(1–6) complex, it is reasonable to propose that the observed decrease in rate of reduction might be ascribed to a decreased driving force for this reaction. Using Marcus semi-classical equation for intermolecular electron transfer, assuming everything else constant, the decreased driving force for the Cu–AS(1–6)M1I complex is expected to decrease its rate of reduction by 26 times, as compared to that of Cu–AS(1–6) (see Supporting Information); however, the experimental value for $k_{ET(AS(1–6))}/k_{ET(AS(1–6)M1I)}$ is 2.4. This analysis indicates that other factors contributing to the rate of reduction of the Cu(II)–AS(1–6) complex are affected by the M1I substitution, and compensate for the decreased driving force. For example, if the reorganization energy associated were to be decreased by 0.23 eV, the predicted ratio of reduction rates $k_{ET(AS(1–6))}/k_{ET(AS(1–6)M1I)}$ would be 2.5, approaching the experimentally determined value (see Supporting Information). Indeed, our electrochemical studies reveal a faster electron transfer kinetics for the M1I variant, as compared to AS(1–6), which could be reflecting a lower reorganization energy for the former. Further spectroscopic and theoretical studies of the reduced form of these complexes would be required to confirm this proposal.

Reoxidation of the Cu(I)–AS(1–6) complexes by oxygen

To evaluate its reactivity with oxygen, the Cu(I)–AS(1–6) complex and its M5I and M1I variants were confronted with oxygen, by adding oxygen-saturated buffer. In all cases, partial recovery of intensity at 610 nm, indicative of reoxidation of the complex, was observed. The reoxidation reaction samples were treated with EDTA to remove the copper ions, and analyzed by HPLC-ESI-TOF (Fig. 5). In all cases, the chromatograms display a peak at retention time of ~31 min (labeled as •), for which the mass spectrometry analysis reveals the presence of the intact peptides with *m/z* values identical to those of the purified peptides (see Table S3). However, the chromatograms reveal the presence of other species. For the AS(1–6) peptide (Fig. 5a), two additional species are observed: one that elutes at $t = 26.1$ min (labeled as *) and displays a m/z corresponding to the peptide with an additional oxygen (Table S3); and a second species with $t = 21.9$ min (labeled as **) and m/z indicative of the addition of two oxygen atoms (Fig. 5b). In contrast, the chromatograms of the M5I and M1I peptides (Fig. 5c, e, respectively) reveal the presence of only one oxidized species: a peak at ~26–27 min (labeled as *) with a *m/z* that corresponds to the peptide with an additional oxygen (Fig. 5d, f, respectively). These results indicate that the peptides that contain only one Met residue (M1I and M5I) get oxidized by one oxygen only, while the AS(1–6) peptide, containing two Met residues, is oxidized by two oxygen atoms. This implies that each Met residue can be oxidized to the sulfoxide form (MetO), while no evidence is observed for their conversion to sulfone species. In the case of the M5I peptide, which contains Met1 only, the extent of oxidation to the sulfoxide form is higher (41.4 %) as compared to that of the M1I peptide (27.5 %), which contains Met5 only (Table S3). These results are consistent with the notion that Met1 is more susceptible to oxidation than Met5, as previously observed by NMR [37]. The higher susceptibility of Met1 towards oxidation is probably due to the fact that this Met residue plays a key role as ligand for both, Cu(II) and Cu(I) ions. Finally, in all cases the ESI-TOF data for the oxidized species reveal a very small peak at a m/z that is indicative of the loss of a CH_3SOH species. These results suggest that the MetO sulfoxide species would be susceptible to an elimination reaction that can generate methanesulfenic acid, and render a peptide with no Met residue, and an alkene moiety instead (Scheme 2). Such an irreversible chemical modification of Met residues 1 and 5 would certainly impair the ability of AS to bind Cu(I) ions.

Copper-catalyzed chemical modifications of the N-terminal region of AS might also have an impact in the folding of AS and its interaction with membranes. Indeed, it has been suggested that oxidation of Met residues favor the formation of toxic AS oligomers, while also affecting the ability of the protein to associate to membranes [39, 70–73]. In the cell, the oxidation of Met residues can be reversed by enzymes, such as methionine sulfoxide reductase (MsrA). However, it was recently shown that, while MsrA can reduce the sulfoxide form of Met5 in AS, it is ineffective in reverting the oxidation of Met1 [74], which is precisely the most susceptible residue to copper-catalyzed oxidation. Furthermore, since the MetO species are susceptible to elimination of sulfenic acid, rendering an alkene moiety, copper-catalyzed oxidation of Met1 in AS would lead to an irreversible chemical modification of the

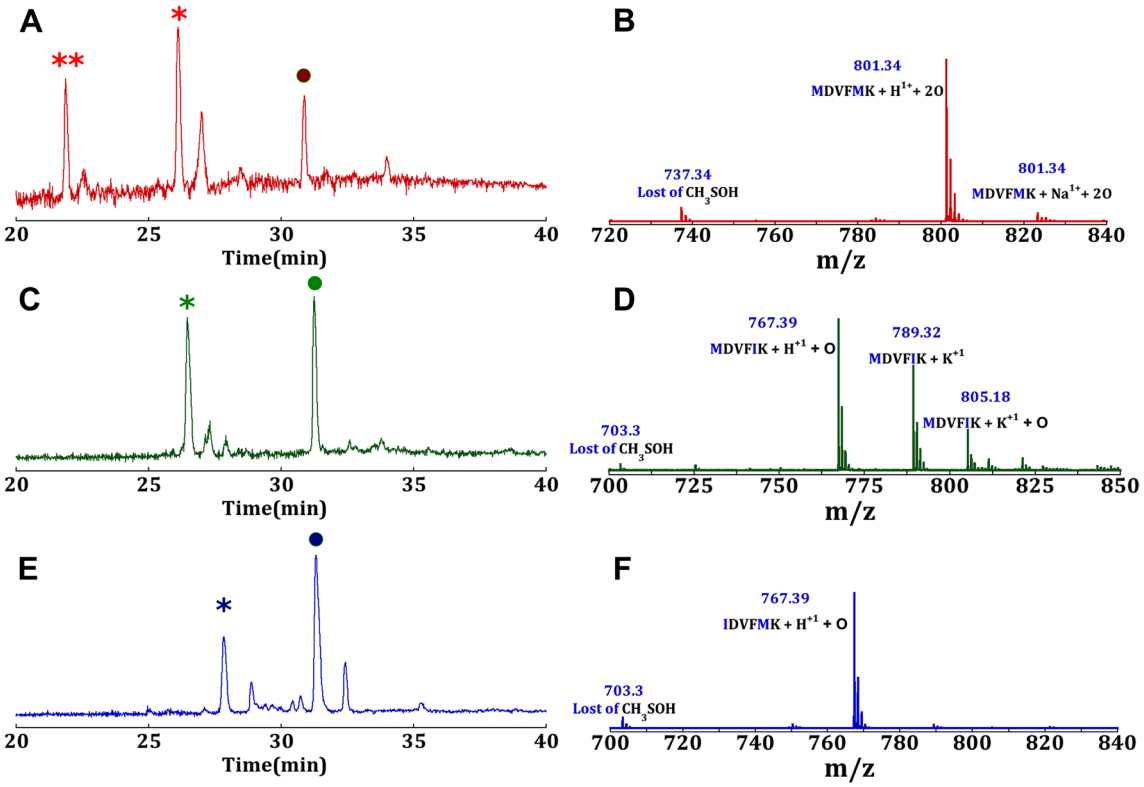

Fig. 5 HPLC-ESI-TOF analysis of AS(1–6) (*red*, **a**), AS(1–6)M5I (*green*, **c**), and AS(1–6)M1I (*blue*, **e**), after one redox cycle with copper; HPLC chromatograms are shown in **a**, **c** and **e**, respectively. The elution peaks labeled as *filled circle* display *m/z* values identical to the non-modified purified peptides (Table S3). ESI-TOF data for the peak labeled *double asterisk* in the AS(1–6) chromatogram is shown in **b**, while ESI-TOF data for the peaks labeled *asterisk* in the M5I and M1I chromatograms are shown in **d** and **f**, respectively. In all cases, the Cu(II):peptide ratio was 0.9:1.0, and the total peptide concentration was 1 mM, using MOPS buffer pH 7.5. A summary of all the species identified by HPLC-ESI-TOF is provided in Table S3

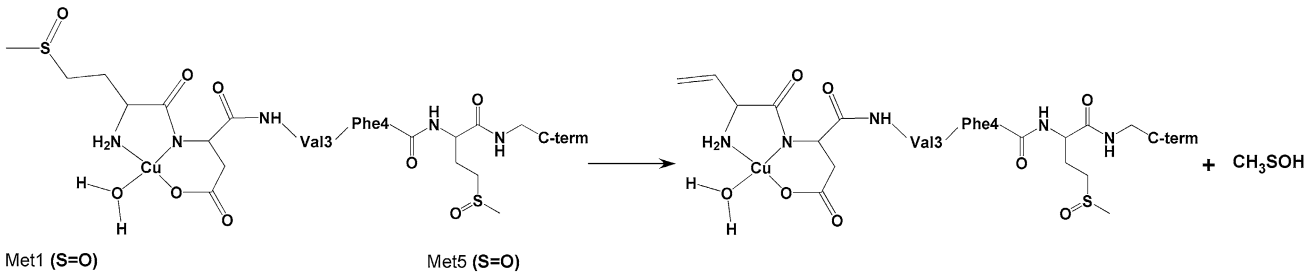

Scheme 2 Copper catalyzed oxidation of AS(1–6) results in a sulfoxide species at both, Met1 and Met5. Subsequent elimination of methanesulfenic acid from the Met1 sulfoxide species renders a peptide with an alkene moiety at this position. This chemical modification would impair the ability of AS to bind Cu(I) ions

N-terminal domain of AS, if Met oxidation at this position cannot be reverted.

Conclusions

In this study, the role of Met1 and Met5 in Cu(II) coordination to the AS(1–6) fragment and the redox activity of the resulting Cu–AS(1–6) complex were evaluated. By combining spectroscopic studies and electronic structure calculations, we show that Met1 may play a role as an axial ligand in the Cu(II)–AS(1–6) complex, while Met5 does not participate in metal coordination at all. Our reactivity studies show that, while both Met residues are important in the reduction and reoxidation of this complex, Met1 plays a more important role than Met5. In contrast to the case of

Met5, substitution of Met1 by Ile causes a drastic decrease in the reduction potential of the Cu–AS(1–6) complex, and consequently, a decrease in the rate of reduction of this complex. The significant contribution of Met1 to the reduction potential and reactivity of the Cu–AS(1–6) complex directly reflects its important role as a ligand for Cu(I). Moreover, we show that Met1 is the most susceptible residue to copper-catalyzed oxidation, and its physiologically irreversible oxidation to sulfoxide could result into a permanent chemical modification that would impair the ability of AS to bind Cu(I) ions. Consequently, copper-catalyzed oxidation of AS may impact the ability of this protein to associate to membranes and it may favor the formation of toxic oligomers of AS. Overall, our study provides a detailed characterization of the copper-catalyzed oxidation of the N-terminal residues of AS, it underscores the important roles that Met1 plays in copper coordination and in the reactivity of the Cu–AS complex.

Acknowledgments This research was funded by CONACYT (Grants 128255 and 221134 to L. Q.). E. E. R., T. A. L. and L. G. T. O. thank CONACYT for Ph.D. fellowships. The authors would also like to thank: I. Q. Geiser Cuellar for assistance with the acquisition of ESI–MS data; and CGSTIC-Cinvestav for providing computing time at "Xiuhcoatl Hybrid Supercomputing Cluster".

References

1. Obeso JA, Rodriguez-Oroz MC, Marin CGGC, Kordower JH, Rodriguez M, Hirsch EC, Farrer M, Schapira AHV, Halliday G (2010) Nat Med 16:653–661
2. Forno LS (1996) J Neuropathol Exp Neurol 55:259–272
3. Goedert M (2001) Nat Rev Neurosci 2:492
4. Spillantini MG, Schmidt ML, Lee VM, Trojanowski JQ, Jakes R, Goedert M (1997) Nature 388:839–840
5. Recchia A, Debetto P, Negro A, Guidolin D, Skaper SD, Giusti P (2004) FASEB J 18:617–626
6. Dexter DT, Wells FR, Lees AJ, Agid F, Agid Y, Jenner P, Marsden CD (1989) J Neurochem 52:1830–1836
7. Maroteaux L, Campanelli JT, Scheller RH (1988) J Neurosci 8:2804–2815
8. Davidson WS, Jonas A, Clayton DF, George JM (1998) J Biol Chem 273:9443
9. Bussell R Jr, Eleizer D (2003) J Mol Biol 329:763
10. Diao J, Burré J, Vivona S, Cipriano DJ, Sharma M, Kyoung M, Südhof TC, Brunger AT (2013) eLife 2:e00592
11. Ischiropoulos H (2003) Ann N Y Acad Sci 991:93–100
12. Hashimoto M, Rockenstein E, Mante M, Mallory M, Masliah E (2001) Neuron 32:213
13. Bertoncini CW, Jung YS, Fernandez CO, Hoyer W, Griesinger C, Jovin TM, Zweckstetter M (2005) Proc Natl Acad Sci USA 102:1430
14. Dedmon MM, Lindorff-Larsen K, Christodoulou J, Vendruscolo M, Dobson CM (2005) J Am Chem Soc 127:476
15. Cho MK, Kim HY, Fernandez CO, Becker S, Zweckstetter M (2011) Protein Sci 2:387–395
16. Fredenburg RA, Rospigliosi C, Meray RK, Kessler JC, Lashuel HA, Eliezer D, Lansbury PT Jr (2007) Biochemistry 46:7107–7118
17. Kang L, Wu K-P, Vendruscolo M, Baum J (2011) J Am Chem Soc 133:13465–13470
18. Lesage S, Anheim M, Letournel F, Bousset L, Honore A, Rozas N, Pieri L, Madiona K, Durr A, Melki R, Verny C, Brice A (2013) Ann Neurol 73:459–471
19. Ghosh D, Mondal M, Mohite GM, Singh PK, Ranjan P, Anoop A, Ghosh S, Jha NN, Kumar A, Maji SK (2013) Biochemistry 52:6925–6927
20. Uversky VN, Li J, Fink AL (2001) J Biol Chem 276:44284–44296
21. Rasia RM, Bertoncini CW, Marsh D, Hoyer W, Cherny D, Zweckstetter M, Griesinger C, Jovin T, Fernández CO (2005) Proc Natl Acad Sci USA 102:4294
22. Binolfi A, Rasia RM, Bertoncini CW, Ceolin M, Zweckstetter M, Griesinger C, Jovin TM, Fernandez CO (2006) J Am Chem Soc 128:9893
23. Iwai A, Masliah E, Yoshimoto N, Ge N, Flanagan L, de Silva HA, Kittel A, Saitoh T (1995) Neuron 14:467
24. Dexter DT, Carayon A, Javoy-Agid F, Agid Y, Wells FR, Daniel SE, Lees AJ, Jenner P, Marsden CD (1991) Brain 114:1953–1975
25. Pall HS, Williams AC, Blake DR, Lunec J, Gutteridge JM, Hall M, Taylor A (1987) Lancet 2:238–241
26. Binolfi A, Lamberto GR, Duran R, Quintanar L, Bertoncini CW, Souza JM, Cerveñansky C, Zweckstetter M, Griesinger C, Fernández CO (2008) J Am Chem Soc 130:11801–11812
27. Binolfi A, Rodriguez EE, Valensin D, D'Amelio N, Ippoliti E, Obal G, Duran R, Magistrato A, Pritsch O, Zweckstetter M, Valensin G, Carloni C, Quintanar L, Griesinger C, Fernandez OC (2010) Inorg Chem 49:10668–10679
28. Valensin D, Camponeschi F, Luczkowski M, Baratto MC, Remelli M, Valensin G, Kozlowski H (2011) Metallomics 3:292–302
29. De Ricco R, Valensin D, Dell'Acqua S, Casella L, Dorlet P, Faller P, Hureau C (2015) Inorg Chem 54:4744–4751
30. Sayre LM, Perry G, Smith MA (2008) Chem Res Toxicol 21:172–188
31. Túnez I, Sánchez-López F, Agüera E, Fernández-Bolaños R, Sánchez FM, Tasset-Cuevas I (2011) J Med Chem 54:5602–5606
32. Varadarajan S, Kanski J, Aksenova M, Lauderback C, Butterfield DA (2001) J Am Chem Soc 123:5625–5631
33. El-Agnaf OMA, Jakes R, Curran MD, Middleton D, Ingenito R, Bianchi E, Pessi A, Neill D, Wallace A (1998) FEBS Lett 440:71–75
34. Winner B, Jappelli R, Maji SK, Desplats PA, Boyer L, Aigner S, Hetzer C, Loher T, Vilar M, Campioni S, Tzitzilonis C, Soragni A, Jessberger S, Mira H, Consiglio A, Pham E, Masliah E, Gage FH, Riek R (2011) Proc Natl Acad Sci 108:4194–4199
35. Turnbull S, Tabner BJ, El-Agnaf OMA, Moore S, Davies Y, Allsop D (2001) Free Radic Biol Med 30:1163–1170
36. Binolfi A, Valiente-Gabioud AA, Duran R, Zweckstetter M, Griesinger C, Fernandez CO (2011) J Am Chem Soc 133:194–196
37. Miotto MC, Rodriguez EE, Valiente-Gabioud AA, Torres-Monserrat V, Binolfi A, Quintanar L, Zweckstetter M, Griesinger C, Fernańdez CO (2014) Inorg Chem 53:4350–4358
38. Lucas HR, Debeer S, Hong MS, Lee JC (2010) J Am Chem Soc 132:6636
39. Uversky VN, Yamin G, Souillac PO, Goers J, Glaser CB, Fink AL (2002) FEBS Letters 517:239–244
40. Glaser CB, Yamin G, Uversky VN, Fink AL (2005) Biochim Biophys Acta 1703:157–169
41. Vogt W (1995) Free Radic Biol Med 18:93–105
42. Levine RL, Berlett BS, Moskovitz J, Mosoni L, Stadtman ER (1999) Mech Ageing Dev 107:323–332
43. Ciorba MA, Heinemann SH, Weissbach H, Brot N, Hoshi T (1997) Proc Natl Acad Sci USA 94:9932–9937

44. Yamin G, Glaser CB, Uversky VN, Fink AL (2003) J Biol Chem 278:27630
45. Miotto MC, Binolfi A, Zweckstetter M, Griesinger C, Fernandez CO (2014) J Inorg Biochem 141:208–211
46. De Ricco R, Valensin D, Dell'Acqua S, Casella L, Gaggelli E, Valensin G, Bubacco L, Mangani S (2015) Inorg Chem 54:265–272
47. Kates EA, Albericio F (2000) Solid-phase synthesis. Marcel Dekker Inc, New York
48. Hood CA, Fuentes G, Patel H, Page K, Menakuru M, Park JH (2008) J Pept Sci 14:97–101
49. Schaftenaar G, Noordik JH (2000) J Comput Aided Mol Des 14:123–134
50. Kohn W, Sham LJ (1965) Phys Rev 140:A1133–A1138
51. Koster AM, Geudtner G, Calaminici P, Casida ME, Dominguez VD, Flores-Moreno R, Gamboa GU, Goursot A, Heine T, Ipatov A, Janetzko F, del Campo JM, Reveles JU, Vela A, Zuniga-Gutierrez B, Salahub DR (2011) deMon2k, version 2: the deMon developers. Cinvestav, Mexico City
52. Dirac PAM (1930) Proc Camb Philos Soc 26:376–385
53. Vosko SH (1980) J Phys 58:1200–1211
54. Perdew JP, Burke K, Ernzerhof M (1996) Phys Rev Lett 77:3865–3868
55. Godbout N, Salahub DR, Andzelm J, Wimmer E (1992) Can J Chem 70:560–571
56. Dunlap BI, Connolly JWD, Sabin JR (1979) J Chem Phys 71:3396–3402
57. Koster AM, del Campo JM, Janetzko F, Zuniga-Gutierrez B (2009) J Chem Phys 130:114106
58. Neese F (2008) ORCA—an ab initio density functional and semiempirical program package, version 26, rev 35. University of Bonn
59. Adamo C, Barone V (1999) J Chem Phys 110:6158
60. The ORCA basis set "CoreProp" was used:this basis is based on the TurboMole DZ basis developed by Ahlrichs and co-workers and obtained from the basis set library under ftp.chemie.uni-karlsruhe.de/pub/basen
61. Klamt A, Schuurmannt G (1993) J Chem Soc Perkin Trans 2:799–805
62. Sinnecker S, Rajendran A, Klamt A, Diedenhofen M, Neese F (2006) J Phys Chem A 110:2235–2245
63. Daniele PG, Prenesti E, Ostacoli G (1996) J Chem Soc Dalton Trans 15:3269–3275
64. Patchkovskii S, Ziegler T (2000) J Am Chem Soc 122:3506–3516
65. Neese F (2003) J Chem Phys 118:3939–3948
66. Rivillas-Acevedo L, Grande-Aztatzi R, Lomeli I, Garcia JE, Barrios E, Teloxa S, Vela A, Quintanar L (2011) Inorg Chem 50:1956–1972
67. Grande-Aztatzi R, Rivillas-Acevedo L, Quintanar L, Vela A (2013) J Phys Chem B 117:789–799
68. Gomez-Castro CZ, Vela A, Quintanar L, Grande-Aztatzi R, Mineva T, Goursot A (2014) J Phys Chem B 118:10052–10064
69. Bard AJ, Faulkner LR (2001) Electrochemical methods: fundamentals and applications, 2nd edn. Wiley, New York
70. Cole NB, Murphy DD, Lebowitz J, Di Noto L, Levine RL, Nussbaum RL (2005) J Biol Chem 280:9678–9690
71. Zhou W, Long C, Reaney SH, Di Monte DA, Fink AL, Uversky VN (2010) Biochim Biophys Acta 1802:322
72. Glaser CB, Yamin G, Uversky VN, Fink AL (2005) Biochim Biophys Acta 1703:157–169
73. Hokenson MJ, Uversky VN, Goers J, Yamin G, Munishkina LA, Fink AL (2004) Biochemistry 43:4621–4633
74. Maltsev AS, Chen J, Levine RL, Bax A (2013) J Am Chem Soc 135:2943–2946